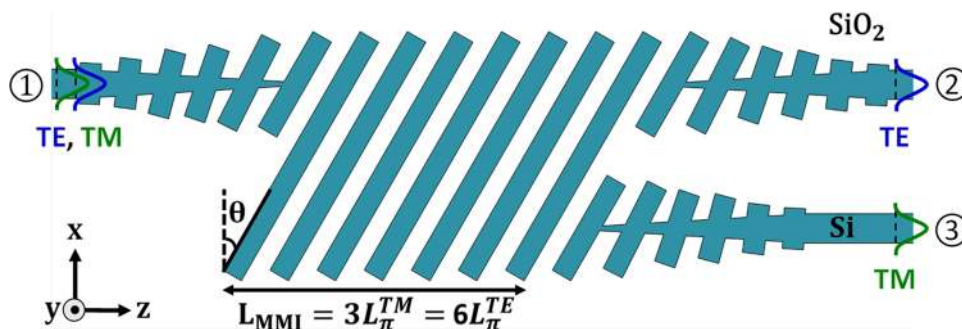# Design of a Broadband Polarization Splitter Based on Anisotropy-Engineered Tilted Subwavelength Gratings

Alaine Herrero-Bermello
José Manuel Luque-González
Aitor V. Velasco
Alejandro Ortega-Moñux
Pavel Cheben
Robert Halir

Design of a Broadband Polarization Splitter Based on Anisotropy-Engineered Tilted Subwavelength Gratings

Alaine Herrero-Bermello [ID],[1] **José Manuel Luque-González** [ID],[2]
Aitor V. Velasco [ID],[1] **Alejandro Ortega-Moñux** [ID],[2]
Pavel Cheben,[3] **and Robert Halir**[2]

[1]Instituto de Óptica, Consejo Superior de Investigaciones Científicas, Madrid 28006, España
[2]Universidad de Málaga, Departamento de Ingeniería de Comunicaciones, ETSI Telecomunicación, Campus de Teatinos s/n, Málaga 29071 España
[3]National Research Council of Canada, Ottawa, ON K1A 0R6, Canada

Abstract: Polarization management is of paramount importance in integrated optics, particularly for highly birefringent photonic platforms such as silicon-on-insulator. In this paper, we present a polarization beam splitter based on a multimode interference coupler incorporating tilted subwavelength gratings. The tilt provides accurate control of the structural anisotropy and enables independent selection of the beat length for two orthogonal polarization states. As a result, device length is reduced to less than 100 μm while simultaneously achieving broadband operation through subwavelength grating dispersion engineering. Insertion losses below 1 dB and an extinction ratio higher than 20 dB are demonstrated through three-dimensional FDTD simulation in a 131-nm bandwidth.

Index Terms: Polarization beam splitter (PBS), multimode interference coupler (MMI), subwavelength grating (SWG), anisotropy engineering, silicon-on-insulator (SOI).

1. Introduction

ON-CHIP polarization management has become an important demand in integrated photonics, especially in highly birefringent platforms such as silicon-on-insulator (SOI). Specifically, polarization beam splitters (PBS) are required for separating the quasi transverse electric (TE) and transverse magnetic (TM) polarization states, ideally with a high extinction ratio (ER) and low insertion losses (IL) over a broad bandwidth [1], [2]. Several different approaches have been proposed to achieve polarization splitting. PBS based on Mach-Zehnder interferometer are straightforward to fabricate, but their bandwidth is generally limited [3]. The bandwidth is also quite limited for two-dimensional gratings couplers (GC) [4], [5], which implement polarization splitting directly at the fiber-chip coupling stage. Directional couplers (DC) have been advantageously used for polarization splitting and can achieve large bandwidths with sophisticated bent designs [1]. DC performance can also be

enhanced through the deposition of additional material layers [6], albeit at the expense of increased fabrication complexity. Other approaches include photonic crystals (PCs) [7], [8], which present more limited ERs and bandwidths, as well as slotted [9] and plasmonic [2] waveguides, which often require multiple fabrication steps.

The properties of subwavelength gratings (SWGs), i.e. spatial arrangements of alternating materials that can be approximated as a homogenous metamaterial [10]-[14], have been exploited to overcome some of the limitations of conventional polarization beam splitters [15]-[18]. For broadband polarization splitting, multimode interference couplers (MMIs) are particularly promising candidates. PBSs based on conventional MMIs have comparatively large footprints [19], [20], which can be reduced by using quasi-imaging [21], photonic crystals [22], slot waveguides [23], metal-insulator-metal structures [24] and augmented-low-index-guiding waveguides [25]. In particular, the inherent anisotropy of SWG enables MMIs with virtually wavelength independent beat lengths for TE polarization, thereby enabling ultra-broad bandwidths. A more detailed description of this anisotropy phenomenon can be found in [26]. Indeed, this concept can be exploited to develop MMIs that act as broadband polarization splitters [27]. Recently, tilted SWGs were proposed as a means to control the anisotropy of the metamaterial, enabling independent engineering of the propagation constants of TE and TM polarized modes [28].

In this paper, we exploit, for the first time, the properties of tilted SWGs to design a broadband polarization splitter, shown in Fig. 1(a), by independently controlling the self-imaging lengths for TE and TM polarization. By using the tilt angle as an additional degree of freedom, we achieve a bandwidth in excess of 131 nm (calculated at IL $<$ 1 dB and ER $>$ 20 dB). Even in the presence of fabrication errors this performance is maintained over the complete C and L bands.

2. Principle of Operation and Design

The operation of an MMI acting as a PBS is illustrated in Fig. 1(b). For each polarization, the fundamental mode of the input waveguide (P1) is launched into the wider central region, exciting higher order modes that mutually interfere as they propagate in the multimode waveguide, forming a self-image of the input field at distances $m(3L_\pi)$, where L_π is the beat length of the two lowest order modes and m is an integer. The beat length is defined as $L_\pi = \pi/(\beta_1 - \beta_2)$ [29], where β_1 and β_2 are the Bloch-Floquet propagation constants of the fundamental and first order modes, respectively, defined as $n_{\mathit{eff},1}2\pi/\lambda$ and $n_{\mathit{eff},2}2\pi/\lambda$.

Images are formed at the through port (P2) for even values of m and at the cross port (P3) for odd values of m. Thus, polarization splitting is achieved if the beat lengths for TE and TM polarization fulfill the condition $(2m^{TM} - 1)L_\pi^{TM} = 2m^{TE}L_\pi^{TE}$. Note that for conventional MMIs (i.e. without SWG structure) the difference between L_π^{TE} and L_π^{TM} is generally small, so that large values of m^{TE} and m^{TM}, and hence very long devices, are required [20]. Furthermore, L_π^{TE} and L_π^{TM} are affected by dispersion, limiting device bandwidth.

In our device design [see Fig. 1(a)] we leverage two properties of SWG structures to overcome these limitations. First, SWG structures behave as equivalent uniaxial crystals [14], defined through the diagonal dielectric tensor $\epsilon = [n_{xx}^2, n_{yy}^2 = n_{xx}^2, n_{zz}^2]$, where n_{xx}, n_{yy} and n_{zz} are the refractive indexes in the x, y and z directions, respectively [30], [31]. This results in a large difference between the beat lengths for TE and TM polarization and allows us to use $m^{TE} = m^{TM} = 1$, thereby minimizing device length. Second, titling the SWG segments with respect to the transversal direction (x) provides direct control over the anisotropy of the equivalent medium. This behavior arises because TE modes are polarized in the x-z plane and thus they perceive a refractive index change from n_{xx} to n_{zz} when the segments rotate from parallel to the x axis ($\theta = 0°$) to parallel to the z axis ($\theta = 90°$). In contrast, TM modes are y-polarized, so they mainly perceive $n_{yy} = n_{xx}$, and are unaffected by the rotation. A more detailed explanation of the anisotropic behavior of tilted SWG structures can be found in [28]. The segments' tilt angle (θ) can then be used to fine-tune the beat length for both polarizations, to fulfill the polarization splitting condition $L_\pi^{TM} = 2L_\pi^{TE}$. Advantageously, the duty cycle of the SWG structure can be kept constant for given fabrication constraints (minimum feature size), while varying the SWG period to optimize device bandwidth.
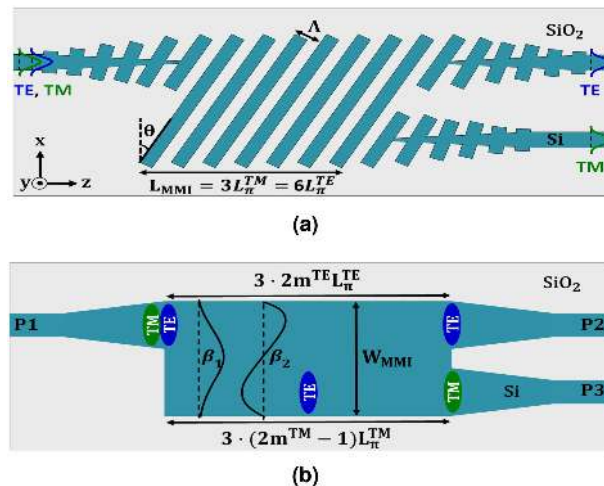
Fig. 1. (a) Polarization beam splitter based on an MMI composed of a tilted subwavelength grating. Metamaterial index engineering by tilting of the SWG segments is used to control the imaging distances for TE and TM polarizations. (b) Schematic principle of operation of an MMI based polarization splitter.

We demonstrate the proposed strategy by designing a high-performance PBS in the silicon-on-insulator platform, for a silicon thickness of 220 nm and single-etch fabrication. The flexibility of our approach in other SOI geometries is illustrated with a further exemplary design for a silicon thickness of 260 nm. We assume thicknesses of the buried oxide (BOX) and upper SiO2 cladding layers of 3 μm and 2 μm, respectively. However, even for the standard SOI 2 μm BOX and a 1 μm silicon dioxide cladding, leakage losses were found to be lower than 0.1 dB in the entire bandwidth. As shown in Fig. 1(a), SWG segments in the multimode region are tilted by an angle θ with respect to the transversal direction (x). The width of the multimode region (W_{MMI}) is 4 μm while its length (L_{MMI}) is given by $N\Lambda/\cos(\theta)$, where N is the number of SWG periods and Λ is the structural period measured perpendicular to the segments. The duty cycle was set at 50% to facilitate the manufacturing process, since it results in a maximization of the minimum feature size of the device; as well as to maintain a good confinement of the TM-polarization mode, avoiding leakage losses. The grating period was set at 220 nm in order to maximize the bandwidth for TE polarization [26], while ensuring that the structure operates in the SWG regime with negligible Bragg reflections. These parameters yield a minimum feature size of 110 nm. Tapers are used in the input and output ports of the multimode region to provide an adiabatic transition between the homogenous waveguides and the tilted SWG region. The width of the taper linearly increases from 1 μm (single mode access waveguides) to a final width of 1.5 μm at the input and output ports. Likewise, the tilt angle θ of the taper SWG segments is gradually varied from 0° to the maximum value in the multimode region. We found that for the designs presented here tapers with 50 periods exhibit negligible losses.

3. Simulation Results

In Fig. 2 we show the MMI lengths at which the TE polarized input mode is imaged to the through port ($6L_\pi^{TE}$), and the TM input is imaged to the cross port ($3L_\pi^{TM}$), for different tilt angles, as a function of the wavelength. In order to obtain accurate results, the beat lengths are calculated from the effective indices of the Bloch modes of the segmented structure, which are obtained using the procedure described in [32]. The circled intersections indicate the points for which the device acts as a polarization splitter. Note that the central wavelength of the device can be tuned by selecting the tilt angle θ, with shorter wavelengths requiring a larger tilt angle. Furthermore, it is observed that the optimum device length for TE polarization is virtually wavelength independent in the 1.45 μm to
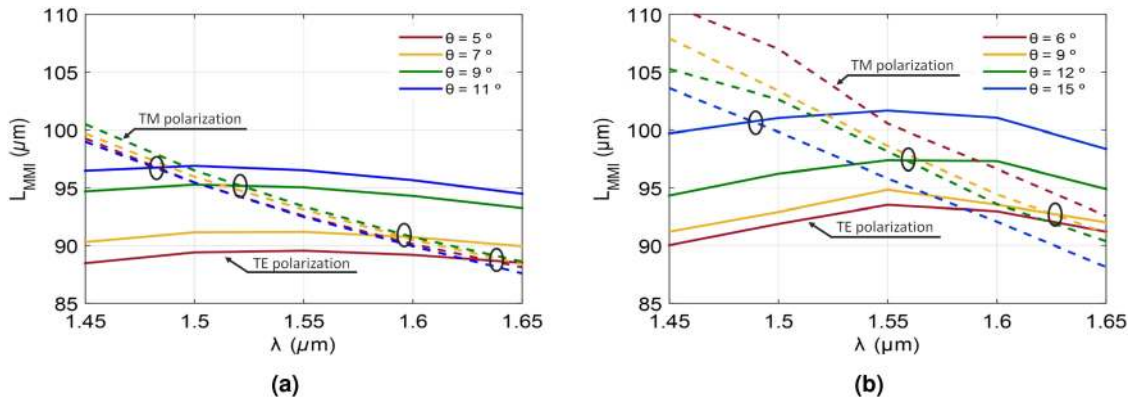
Fig. 2. MMI length as a function of wavelength for TE and TM polarizations and different tilt angles of the SWG segments, for silicon thicknesses of (a) 220 nm and (b) 260 nm. The circled intersections correspond to MMIs operating as a polarization splitter.

1.65 μm band, for all angles and for both 220 nm and 260 nm silicon thicknesses, enabling a broader bandwidth for this polarization. In contrast, the optimum device length for TM modes decreases with wavelength, ultimately limiting the bandwidth of the device. Near the telecom wavelength of 1.55 μm, the condition for polarization splitting is obtained for a tilt angle between 7° and 9° for a silicon thickness of 220 nm and between 12° and 15° for 260 nm.

For the PBS on 220-nm-thick silicon both the tilt angle and the number of periods were further optimized through iterative 3D - FDTD simulations. The final design has a tilt angle of 7° and a length of 92.4 μm, comprising 417 periods with a pitch of 220 nm. The simulations were carried out without any approximations (using the full tilted SWG structure) in a 3D Finite Difference Time Domain (FDTD) simulator [33]. The simulation window was 5.6 μm wide in x direction and 2.8 μm high in y direction, with a grid of 90 nm, 17 nm and 11 nm, in the x, y, and z directions, respectively. We checked that since the device is relatively wide, a relaxed grid can be used in the x-direction, as long as the grid in the y and z directions is sufficiently small to properly sample the tilted segments. The calculated electric field distributions in the MMI polarization beam splitter are shown in Fig. 3. In the upper middle panel, the fundamental TE mode excites the input port (P1) and forms a direct image at a distance $6L_\pi^{TE}$, where the through-port (P2) is located. In the lower middle panel, the fundamental TM mode launched at the input port forms an inverted image at a distance $3L_\pi^{TM}$, where the cross-port (P3) is positioned. The field distributions at the input and output ports, are shown in the left and right panels of the Fig. 3, respectively. The overlap of the electric field at each output with the fundamental TE/TM waveguide mode yields $P_{P2}^{TE} = 0.94$ and $P_{P3}^{TM} = 0.9$. The polarization purity $(P_{P2}^{TE} - P_{P2}^{TE->TM})/P_{P2}^{TE}$ and $(P_{P3}^{TM} - P_{P3}^{TM->TE})/P_{P3}^{TM}$ is virtually 100% for both polarizations, i.e. the device introduces negligible polarization rotation.

The calculated IL and ER for TE and TM polarizations are shown in Fig. 4. The IL are calculated as $10\log(P_{in}^{TE}/P_{P2}^{TE})$ and $10\log(P_{in}^{TM}/P_{P3}^{TM})$, while the ER is $10\log(P_{P2}^{TE}/P_{P3}^{TE})$ and $10\log(P_{P3}^{TM}/P_{P2}^{TM})$, for TE and TM polarizations respectively. The power in the different ports is obtained by overlapping the total electric field with the profile of the fundamental waveguide mode. The results, shown in Fig. 4(a) and Fig. 4(b), demonstrate the broadband performance of the PBS: the response of the device is approximately centered at 1.55 μm, IL are below 1 dB and ER is better than 20 dB for both polarizations in a 131-nm-wide bandwidth (between 1.504 μm and 1.635 μm). At the central wavelength of 1.55 μm, the IL and ER are 0.32 dB and 36.4 dB for TE and 0.51 dB and 35.2 dB for TM polarization. The device bandwidth is limited by the TM response, which is expected given the flatter response of the beat length for TE polarization, as shown in Fig. 2(a). The performance of the optimized device (220-nm-thick SOI) presented in this work is compared to the simulated performance of state-of-the-art PBS in Table 1.
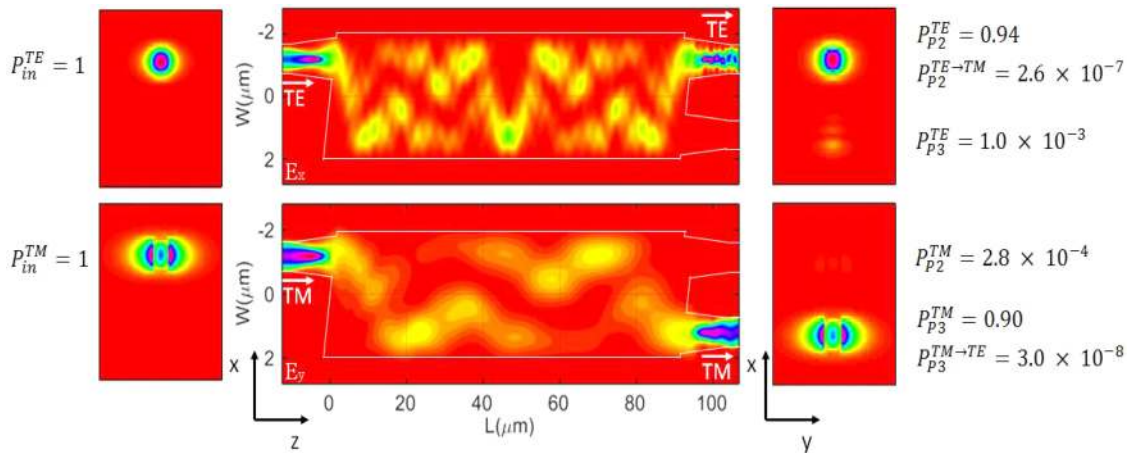
Fig. 3. E_x and E_y components of the electric field, as obtained with 3D FDTD simulations of the full subwavelength structured device. TE propagating along the MMI polarization splitter is shown in the upper middle panel, and the TM propagation in the lower middle panel, both at a wavelength of 1.55 μm and for a silicon thickness of 220 nm. The outline of the device is shown in white contour; for clarity the individual subwavelength periods are not shown. The panels on the left and the right show the electric field distributions at the input and output ports respectively. The overlap of the electric field at the output ports with the fundamental TE/TM waveguide modes is given by $P_{Pi}^{TE/TM}$.
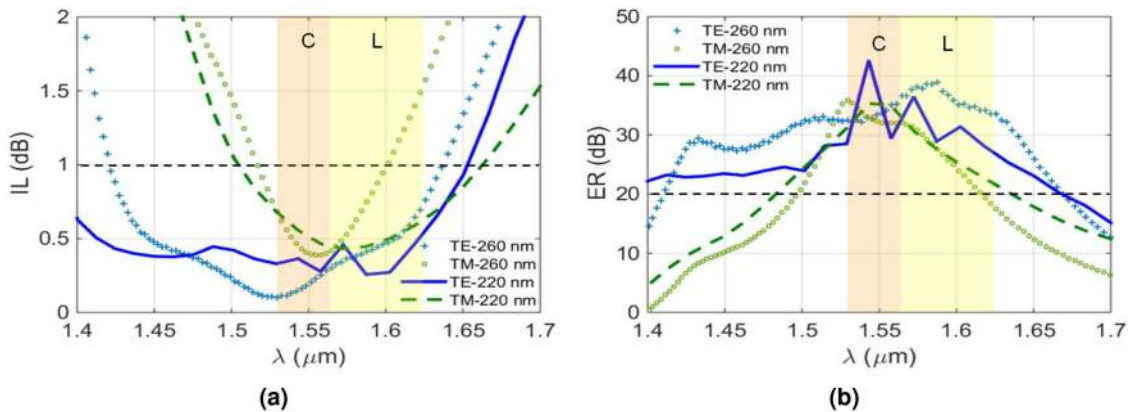

Fig. 4. IL (a) and ER (b) for TE and TM polarizations as a function of the wavelength, for both a silicon waveguide thickness of 220 nm and 260 nm. C and L are the communication bands with a wavelength range of 1.530–1.565 μm and 1.565-1.625 μm respectively.

In order to investigate the versatility of our design strategy, the design procedure described above was carried out also for a 260-nm-thick silicon layer, using a calculated tilt angle of 12°. For this case, the optimized device length for the same central wavelength is 95.1 μm, that is 423 periods with a pitch of 220 nm. The IL remain below 0.6 dB for TE and 1.5 dB for TM within a 116 nm-bandwidth, while the ER exceeds 30 dB and 20 dB for TE and TM polarizations, respectively, demonstrating that our strategy can be applied to different silicon platforms.

Finally, we analyzed the robustness to fabrication errors of our optimized PBS device, for a silicon thickness of 220 nm, by using 3D FDTD simulations (see Fig. 5). Since the duty cycle is expected to be the most critical parameter [26], it was varied between 40% and 60%, resulting in a ± 22 nm variation in the length of the SWG segments. As expected, for the above definition of device bandwidth (ER > 20 dB and IL < 1 dB), the response of the device becomes significantly worse for duty cycles of 40% and 60%, with a reduction of bandwidth of more than 60%. Fig. 5 presents

TABLE 1

Simulated Performance of State-of-the-Art Polarization Splitters and Comparison With the Optimized Device Presented in this Work (Silicon Layer of 220 nm Height, Pitch of 220 nm Wide, Duty Cycle of 50%, Tilt Angle of 7° and 417 Periods). (*Data Estimated From Figures)

| Structure	ER (dB)	IL (dB)	BW (nm)	L (μm)	Ref.
Bent DC	>20	<1	135	20	[1]
Plasm. Wg	<19	<1	400	0.9	[2]
2D GC	>22	<3	70	10	[4]
Asymm. DC	>10	<0.6	100	6.5	[6]
Slotted Wg	<21.8	<1	100	33	[9]
SWG DC	>10	<1	115	21	[15]
SWG DC	>18	<0.7	81	6.8	[17]
Inv. design	<13*	<1	83	2.4	[18]
Conv. MMI	<20	<1	35	1085	[19]
Conv. MMI	>15	N/A	35	1034	[20]
Conv. MMI	>15	<2.2*	41	132.6	[21]
PC MMI	<20	<2	100	50	[22]
Slotted MMI	13	0.3	N/A	48.3	[23]
MIM MMI	12.6	<1.1	N/A	44	[24]
Asym. MMI	>18	<0.4	35	4.8	[25]
SWG MMI	>20	<1.2	95	92.7	[27]
This work	>20	<1	131	92.4	-
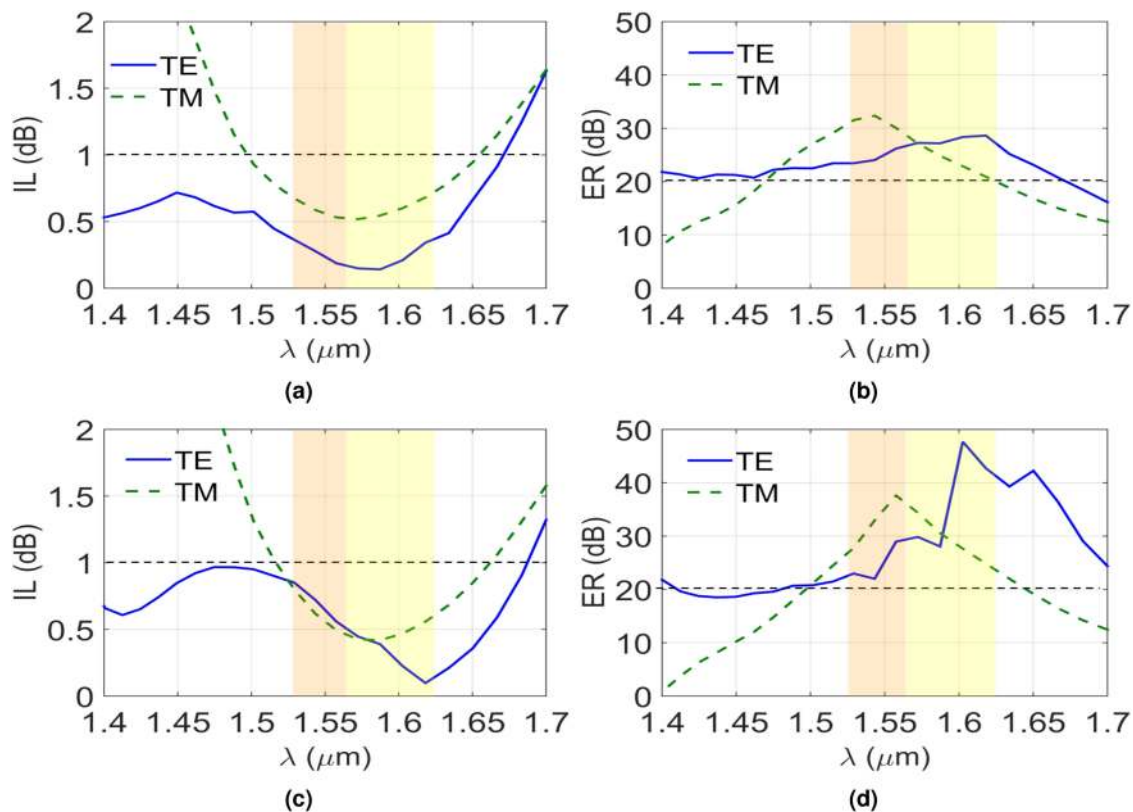
Fig. 5. IL and ER of the 220 nm Si thick PBS for a duty cycle of (a, b) 0.45 and (c, d) 0.55 for TE and TM polarizations. Bandwidth is defined at ER better than 20 dB and IL better than 1 dB.

a detailed IL and ER response to duty cycles of 45% (a and b panels) and 55% (c and d panels), which corresponds to a fabrication error of $\pm$ 11 nm in the length of the segments. For a duty cycle of 45%, the device still presents a large bandwidth of 128 nm (between 1.497 μm and 1.625 μm) with a displacement of the central wavelength of less than 10 nm with respect to the nominal design (131 nm-wide bandwidth between 1.504 μm and 1.635 μm). For the 55% duty cycle, the resulting bandwidth remains close to its nominal value, covering 130 nm (between 1.516 μm and 1.646 μm) with a central wavelength offset of 12 nm. Therefore, even in the presence of fabrication errors in the duty cycle of the order of $\pm$ 5%, the bandwidth is remarkably constant and larger than 128 nm, resulting in full coverage of the C + L communication bands. The tolerance of the device to errors in the width ot the MMI has also been studied, demonstrating that the bandwidth remains over 120 nm even in the presence of MMI width variations of $\pm$ 20 nm.

4. Conclusion

In conclusion, we have proposed a new type of integrated polarization splitter based on waveguide anisotropy, engineering through tilted subwavelength gratings. This new strategy of birefringence control in planar waveguides was applied to a design of a multimode interference coupler with a tilted subwavelength grating, achieving an extinction ratio over 20 dB and insertion losses below 1 dB in a 131-nm-wide bandwidth. Tilting the subwavelength grating allows us to adjust the beat length of both polarizations, minimizing the length of the multimode region, while providing broadband operation. Furthermore, the additional degree of design freedom provided by the grating tilt allows to increase the minimum feature size to 110 nm, compatible with wafer-scale deep-UV lithography. This outstanding design performance, along with the ease of implementation, one-step fabrication and resilience to fabrication errors, make our device a competitive alternative to state-of-the-art nanophotonic polarization beam splitter devices.

Acknowledgment

References

[1] H. Wu, Y. Tan, and D. Dai, "Ultra-broadband high-performance polarizing beam splitter on silicon," *Opt. Exp.*, vol. 25, no. 6, pp. 6069–6075, Mar. 2017.

[2] K.-W. Chang and C.-C. Huang, "Ultrashort broadband polarization beam splitter based on a combined hybrid plasmonic waveguide," *Sci. Rep.*, vol. 6, Jan. 2016, Art. no. 19609.

[3] T. K. Liang and H. K. Tsang, "Integrated polarization beamsplitter in high index contrast SOI waveguide," *IEEE Photon. Technol. Lett.*, vol. 17, no. 2, pp. 393–395, Feb. 2005.

[4] Y. Tang, D. Dai, and S. He, "Proposal for a grating waveguide serving as both a polarization splitter and an efficient coupler for silicon-on-insulator nanophotonic circuits," *IEEE Photon. Technol. Lett.*, vol. 21, no. 4, pp. 242–244, Feb. 2009.

[5] D. Taillaert, H. Chong, P. Borel, L. Frandsen, R. M. De La Rue, and R. Baets, "A compact two-dimensional grating coupler used as a polarization splitter," *IEEE Photon. Technol. Lett.*, vol. 15, no. 9, pp. 1249–1251, Aug. 2003.

[6] C.-W. Hsu, T.-K. Chang, J.-Y. Chen, and Y.-C. Cheng, "8.13 μm in length and CMOS compatible polarization beam splitter based on an asymmetrical directional coupler," *Appl. Opt.*, vol. 55, no. 12, pp. 3313–3318, Apr. 2016.

[7] E. Schonbrum, Q. Wu, and W. Park, "Polarization beamsplitter based on a photonic crystal heterostructure," *Opt. Lett.*, vol. 31, no. 21, pp. 3104–3106, Nov. 2006.

[8] X. Ao, L. Liu, L. Wosinski, and S. He, "Polarization beam splitter based on a two-dimensional photonic crystal of pillar type," *Appl. Phys. Let.*, vol. 89, Oct. 2006, Art. no. 171115.

[9] W. Jiang, X. Sun, and B. A. Rahman, "Compact and fabrication-tolerant polarization splitter based on horizontal triple-slot waveguide," *Appl. Opt.*, vol. 56, no. 8, pp. 2119–2126, Mar. 2017.

[10] R. Halir *et al.*, "Waveguide sub-wavelength structures: A review of principles and applications," *Laser Photon. Rev.*, vol. 9, no. 1, pp. 25–49, Jan. 2015.

[11] P. Cheben *et al.*, "Refractive index engineering with subwavelength gratings for efficient microphotonic couplers and planar waveguide multiplexers," *Opt. Lett.*, vol. 35, no. 15, pp. 2526–2528, Aug. 2010.

[12] P. Cheben, D.-X. Xu, S. Janz, and A. Densmore, "Subwavelength waveguide grating for mode conversion and light coupling in integrated optics," *Opt. Exp.*, vol. 14, no. 11, pp. 4695–4702, May 2006.

[13] P. J. Bock *et al.*, "Subwavelength grating periodic structures in silicon-on-insulator: A new type of microphotonic waveguide," *Opt. Exp.*, vol. 18, no. 19, pp. 20251–20262, Sep. 2010.

[14] P. Cheben, R. Halir, J. Schmid, H. Atwater, and D. Smith, "Subwavelength integrated photonics," *Nature*, vol. 560, pp. 565–572, Aug. 2018.

[15] L. Liu, Q. Deng, and Z. Zhou, "Manipulation of beat length and wavelength dependence of a polarization beam splitter using a subwavelength grating," *Opt. Lett.*, vol. 41, no. 21, pp. 5126–5129, Nov. 2016.

[16] S. Chen, H. Wu, and D. Dai, "High extinction-ratio compact polarization beam splitter on silicon," *Electron. Lett.*, vol. 52, no. 12, pp. 1043–1045, Jun. 2016.

[17] Y. Xu and J. Xiao, "Compact and high extinction ratio polarization beam splitter using subwavelength grating couplers," *Opt. Lett.*, vol. 41, no. 4, pp. 773–776, Feb. 2016.

[18] B. Shen, P. Wang, R. Polson, and R. Menon, "An integrated-nanophotonics polarization beamsplitter with 2.4 x 2.4 μm^2 footprint," *Nature Photon.*, vol. 9, no. 6, pp. 378–382, May 2015.

[19] J. M. Hong *et al.*, "Design and fabrication of a significantly shortened multimode interference coupler for polarization splitter application," *IEEE Photon. Technol. Lett.*, vol. 15, no. 1, pp. 72–74, Jan. 2003.

[20] Y. Huang, Z. Tu, H. Yi, Y. Li, X. Wang, and W. Hu, "High extinction ratio polarization beam splitter with multimode interference coupler on SOI," *Opt. Commun.*, vol. 307, pp. 46–49, Oct. 2013.

[21] M. Yin, W. Yang, Y. Li, X. Wang, and H. Li, "CMOS-compatible and fabrication-tolerant MMI-based polarization beam splitter," *Opt. Commun.*, vol. 335, pp. 48–52, Jan. 2015.

[22] Y. Shi, D. Dai, and S. He, "Proposal for an ultracompact PBS based on a photonic-crystal-assisted MMI coupler," *IEEE Photon. Technol. Lett.*, vol. 19, no. 11, pp. 825–827, May 2007.

[23] A. Katigbak, J. F. Strother, Jr., and J. Lin, "Compact silicon slot waveguide polarization splitter," *Opt. Eng.*, vol. 48, no. 8, Aug. 2009, Art. no. 080503.

[24] V. Chheang *et al.*, "Compact polarizing beam splitter based on a metal-insulator-metal inserted into multimode interference coupler," *Opt. Exp.*, vol. 21, no. 18, pp. 20880–20887, Sep. 2013.

[25] X. Sun, J. S. Aitchison, and M. Mojahedi, "Realization of an ultra-compact polarization beam splitter using asymmetric MMI based on silicon nitride/silicon-on-insulator platform," *Opt. Exp.*, vol. 25, no. 7, pp. 8296–8305, Mar. 2017.

[26] R. Halir *et al.*, "Ultrabroadband nanophotonic beamsplitter using an anisotropic SWG material," *Laser Photon. Rev.*, vol. 10, no. 6, pp. 1039–1046, Nov. 2016.

[27] L. Xu *et al.*, "Polarization beam splitter based on MMI coupler with SWG Birefringence engineering on SOI," *IEEE Photon. Technol. Lett.*, vol. 30, no. 4, pp. 403–406, Jan. 2018.

[28] J. M. Luque-González *et al.*, "Tilted subwavelength gratings: Controlling anisotropy in a metamaterial," *Opt. Lett.*, vol. 43, no. 19, pp. 4691–4694, Sep. 2018.

[29] L. B. Soldano and E. C. M. Pennings, "Optical multi-mode interference devices based on self-imaging: Principles and applications," *J. Lightw. Technol.*, vol. 13, no. 4, pp. 615–627, Apr. 1995.

[30] R. E. Newnham, *Properties of Materials: Anisotropy, Symmetry, Structure*. London, U.K.: Oxford Univ Press, 2005.

[31] A. Yariv and P. Yeh, *Optical Waves in Crystals: Propagation and Control of Laser Radiation*. Hoboken, NJ, USA: Wiley, 1984.

[32] J. G. Wangüemert-Pérez *et al.*, "Evanescent field waveguide sensing with subwavelength grating structures in silicon-on-insulator," *Opt. Lett.*, vol. 39, no. 15, pp. 4442–4445, Jul. 2014.

[33] "FullWAVE," RSoft, 2018. [Online]. Available: http://www.rsoftdesign.com